Thermally Forced Transients in the Thermohaline Circulation

MICHAEL A. SPALL

Woods Hole Oceanographic Institution, Woods Hole, Massachusetts

ABSTRACT

The response of a convective ocean basin to variations in atmospheric temperature is explored using numerical models and theory. The results indicate that the general behavior depends strongly on the frequency at which the atmosphere changes relative to the local response time to air–sea heat flux. For high-frequency forcing, the convective region in the basin interior is essentially one-dimensional and responds to the integrated local surface heat flux anomalies. For low-frequency forcing, eddy fluxes from the boundary current into the basin interior become important and act to suppress variability forced by the atmosphere. A theory is developed to quantify this time-dependent response and its influence on various oceanic quantities. The amplitude and phase of the temperature and salinity of the convective water mass, the meridional overturning circulation, the meridional heat flux, and the air–sea heat flux predicted by the theory compare well with that diagnosed from a series of numerical model calculations in both strongly eddying and weakly eddying regimes. Linearized analytic solutions provide direct estimates of each of these quantities and demonstrate their dependence on the nondimensional numbers that characterize the domain and atmospheric forcing. These results highlight the importance of mesoscale eddies in modulating the mean and time-dependent ocean response to atmospheric variability and provide a dynamical framework with which to connect ocean observations with changes in the atmosphere and surface heat flux.

1. Introduction

The North Atlantic meridional overturning circulation (MOC) transports heat poleward and freshwater equatorward and as such plays an important role in the climate system. The marginal seas of the North Atlantic, such as the Labrador Sea, the Norwegian Sea, and the Greenland Sea, are very important locations for this water mass transformation and, along with entrainment downstream of the Greenland–Iceland–Scotland Ridge, provide the dominant downwelling regions for the MOC (Marshall and Schott 1999).

These basins may be described as regions of closed geostrophic contours (lines of constant f/h, where f is the Coriolis parameter and h is the bottom depth) in the basin interior where deep convection occurs with regions of open geostrophic contours around the basin perimeter. It has been shown that mesoscale eddies play a key role in connecting these two regions and in controlling the mean properties of the water masses produced in the marginal seas (Khatiwala and Visbeck 2000; Lilly and Rhines 2002; Lilly et al. 2003; Spall 2004; Straneo 2006; Spall 2012).

The MOC varies on a wide range of time scales and its variability is likely forced by many different processes. In general, this variability may result from changes in atmospheric forcing, internal variability arising from ocean dynamics, or coupled modes between the ocean and atmosphere. Because of this complexity, it is difficult to sort out what causes observed changes in ocean properties such as temperature and salinity or in ocean circulation such as the MOC. It is tempting to try to correlate changes in the atmosphere, such as winds or temperature, with changes in the ocean observed at a later time or in a different location. However, the observed time series are so short that this is difficult to do on interannual-to-decadal time scales with much statistical significance, and there is currently lacking a sufficient theoretical framework with which to interpret the limited observations.

There have been a number of idealized numerical and theoretical studies aimed at understanding the ocean response to time-dependent forcing. Much of the ocean response can be characterized as an adiabatic adjustment

Corresponding author address: Michael Spall, Woods Hole Oceanographic Institute, MS 21, 360 Woods Hole Road, Woods Hole, MA 02543.
E-mail: mspall@whoi.edu

achieved by westward propagation of Rossby waves in the open ocean and eastward propagation of Kelvin waves along the equator (Kawase 1987). This can arise due to variations in wind stress (Anderson and Killworth 1977; Spall and Pickart 2003) or variations in surface buoyancy flux (Pedlosky 2006). If there is sufficient dissipation along the western boundary, these anomalies are confined to the latitude of forcing, but for weakly damped systems basin-scale modes can be excited (Cessi and Otheguy 2003).

Many more complete general circulation models have also been used to study both internal and externally forced transients in the MOC. Lucas et al. (2005) studied the MOC response to periodic atmospheric temperature variations with periods of 6 months to 32 000 yr in a low-resolution, flat bottom, idealized ocean basin. They found a strong response with a resonancelike behavior for periods longer than 15 yr. Delworth and Greatbatch (2000) used a low-resolution but otherwise realistic global model to show that the dominant variability of the MOC was externally forced by changes in air–sea heat fluxes. Grégorio et al. (2015) came to a similar conclusion, particularly at high latitudes, with an eddy-resolving Atlantic sector general circulation model forced by realistic atmospheric fluxes.

These results motivate a more focused study on the ocean response to variations in atmospheric temperature and thus also surface heat flux. The present study addresses the response of a convective basin, such as the Labrador Sea or the Nordic Seas, to changes in atmospheric temperature. This differs from the study of Lucas et al. (2005) by explicitly resolving mesoscale eddies and by having topography that defines a region of closed geostrophic contours, which is an important feature for the establishment of realistic deep convection. Change in atmospheric temperature is only one element of what is in reality a much more complicated and widely connected system. However, by simplifying the problem we are able to construct analytically tractable models and provide an estimate based on theory for how the amplitude and phase of the key elements of the buoyancy-forced thermohaline circulation respond to such external forcing.

2. A simple time-dependent model of a convection region

Following Spall (2012) and Yasuda and Spall (2015), a simple model is now developed to represent the gross characteristics of the water mass properties and transports associated with deep convection. The model consists of two regions: an interior where deep convection takes place and a buoyant cyclonic boundary current that flows around the deep convection site (see the appendix). This describes, in a very general way, the circulation in the vicinity of convective sites in the Labrador Sea, the

Greenland Sea, the Lofoten basin, and the Mediterranean Sea (Marshall and Schott 1999). The dependent variables are the differences in temperature and salinity between the boundary current and the convection site or the temperature and salinity anomalies of the convective water relative to the boundary current. It is assumed that the temperature and salinity flowing into the basin in the boundary current, T_1 and S_1, are known and the same as that found along the eastern boundary outside the marginal sea. The model is forced by a surface heat flux given by $Q = \Gamma(T - T_a)$, where Γ is a restoring constant with units $\mathrm{W\,m^{-2}\,(°C)^{-1}}$, T is the ocean temperature, and T_a is the atmospheric temperature. This introduces a natural temperature scale with which to nondimensionalize temperature as $T^* = T_1 - \overline{T}_a$, where $\overline{T}_a$ is now the mean atmospheric temperature. Salinity (S) is scaled by the salinity difference that gives the same density change as T^*: $\alpha_T T^*/\alpha_S$, where α_T and α_S are the thermal and haline contraction coefficients. It is assumed that the atmospheric temperature is spatially constant, but it will be allowed to vary in time. Salinity is forced by a spatially and temporally uniform surface virtual freshwater flux over the marginal sea.

a. Temperature and salinity of the convective water mass

The model is a time-dependent extension of the steady-state model described by Spall (2012). A similar set of equations was also analyzed by Yasuda and Spall (2015) subject to time-dependent precipitation. A brief summary of the derivation is given in the appendix, and a more detailed derivation can be found in Yasuda and Spall (2015). The nondimensional difference between the temperature in the boundary current and the temperature in the basin interior is ΔT, and the nondimensional salinity difference is ΔS. A value of ΔT or ΔS of zero means that the temperature or salinity of the convective interior is the same as that of the inflowing boundary current. The atmospheric temperature is spatially uniform but varies sinusoidally in time with nondimensional amplitude T' and frequency ω. The governing nondimensional equations are

$$\frac{d\Delta T}{dt} = -\Delta T(\Delta T - \Delta S) + 2\mu/\epsilon[1 - \Delta T + T'\sin(\omega t)],$$

(1a)

and

$$\frac{d\Delta S}{dt} = -\Delta S(\Delta T - \Delta S) - \gamma/4\epsilon.$$

(1b)

The time-dependent $\Delta T = \Delta T_0 + \delta T$ and $\Delta S = \Delta S_0 + \delta S$ can be written as the sum of the steady solution ΔT_0 and ΔS_0 (with $T' = 0$) and variations due to T', δT, and δS.
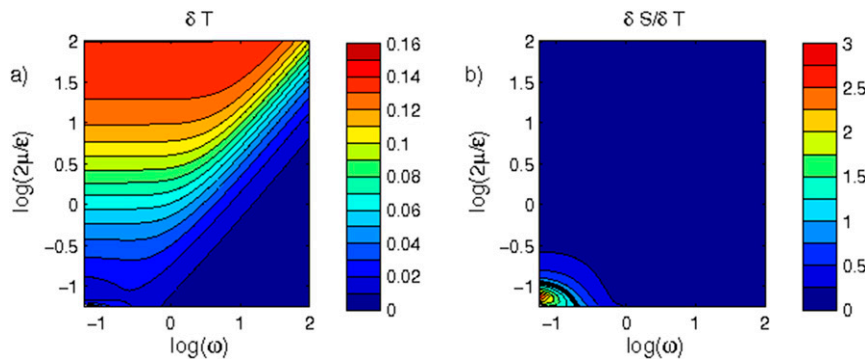
FIG. 1. (a) Nondimensional amplitude of variance in temperature of the convective water mass as a function of forcing frequency ω and relative importance of eddies (eddies are strong when $2\mu/\epsilon \ll 1$). Atmospheric temperature varies sinusoidally with amplitude 0.14. (b) Ratio of salinity variance to temperature variance.

As discussed by Spall (2012), these equations are similar to those in the two-box model of Stommel (1961), but the physical interpretation is somewhat different. In the Stommel model, the exchange between boxes is a result of a mean flow down the pressure gradient, and in the present model the exchange is driven by eddy fluxes down the pressure gradient while the mean flow is geostrophic and parallel to pressure contours. The exchange between boxes in Stommel's model represents the downwelling forced by cooling in the northern box, while the exchange here is the diapycnal mass flux, generally not all vertical. The net downwelling is calculated below, and it will be seen that this is different from, and generally smaller than, the diapycnal mass flux.

Equation (1) can be integrated numerically to solve for ΔT and ΔS as a function of time. The amplitude of the variation in the temperature and salinity of the convective water mass diagnosed from such integrations is shown in Fig. 1 as a function of the forcing frequency ω and the parameter measuring the strength of eddy heat fluxes between the boundary and the interior $2\mu/\epsilon$ (see the appendix). For this case, $T^* = 7°C$ and the temperature is varied sinusoidally by $1°C$, giving a nondimensional variation of $T' = 0.14$. For very low-frequency forcing and weak eddy fluxes ($2\mu/\epsilon \gg 1$), the amplitude of the variation in temperature is simply given by the nondimensional T'. As the boundary current becomes more unstable, or the restoring to the atmosphere weakens, $2\mu/\epsilon$ decreases and the amplitude of the temperature variability decreases. For very strong eddies ($2\mu/\epsilon \ll 1$), the temperature varies by an order of magnitude less than the variation in atmospheric temperature. This is because the eddy fluxes from the boundary current are so strong that they quickly compensate for the change in atmospheric temperature by pulling the water mass back toward the temperature of

the boundary current. The temperature variation is greatly reduced for all values of $2\mu/\epsilon$ as the frequency of forcing is increased. This transition from large variability to small variability occurs for a frequency of approximately $2\mu/\epsilon$, although the transition occurs gradually over an order of magnitude in ω. In dimensional units, this transition frequency is simply $\Gamma/\rho_0 C_p H_0$, which is the local response time for the full-depth basin to respond to atmospheric forcing. For a restoring constant of $\Gamma = 10\,\mathrm{W\,m^{-2}\,(°C)^{-1}}$ and a convective basin depth of $1500\,\mathrm{m}$, this gives a frequency of $1.6 \times 10^{-9}\,\mathrm{s^{-1}}$ or a period of approximately $3\,\mathrm{yr}$. At frequencies higher than this the convective basin is essentially one-dimensional; the sign of the forcing changes before the boundary current has been able to flux a significant amount of heat into the basin interior. The salinity variability is nearly always much less than the temperature variability, as shown in Fig. 1b. The exception is for strong eddy fluxes and low-frequency forcing, in which case the salinity variability becomes larger than the temperature variability. This will be discussed further below.

It is of interest to understand not only how strongly the ocean responds to changes in the atmospheric temperature but also when the ocean responds or what the phase of the ocean is compared to the phase of the atmospheric temperature anomaly. The phase of T_0 and S_0, the properties of the convective water mass, is shown in Fig. 2. The convention is such that the phase is zero if the temperature of the convective water mass is warm or the salinity is high when the atmosphere is warm, and the phase is negative when the ocean lags the atmosphere. Temperature is in phase with the atmosphere at low frequency and lags the atmosphere by $90°$ at high frequency. Once again, the transition from low to high frequency occurs when $\omega = 2\mu/\epsilon$. The in-phase response at low frequency is consistent with the ocean being
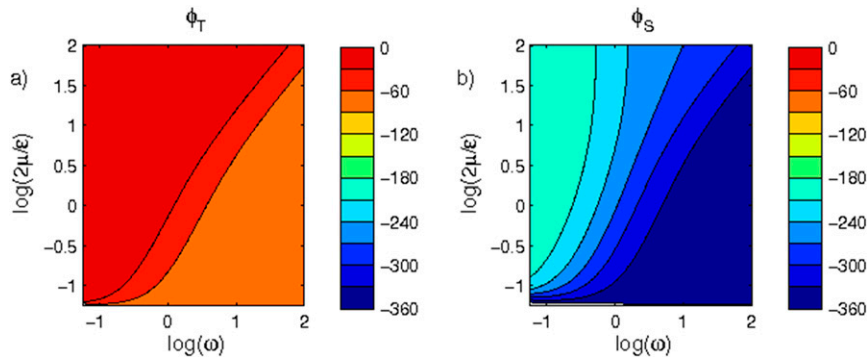
FIG. 2. Phase relationship between convective water mass (a) temperature and (b) salinity relative to atmospheric temperature.

nearly in balance with the atmosphere at all times, slowly following the anomalous forcing. The lag at high frequencies is such that the ocean is warmest at the end of the anomalously warm atmosphere, as would be expected for a one-dimensional response. Salinity transitions from being 180° out of phase at low frequency to in phase at high frequency. The convective water mass is fresh when the atmosphere is warm. This is because a warm atmosphere, and thus a warm ocean interior, reduces the baroclinic shear of the boundary current (because the horizontal density gradient is reduced) and thus the strength of the lateral salt flux into the interior carried by eddies. The precipitation is constant in time, and so the salinity of the convective water mass decreases.

b. Meridional heat transport and overturning circulation

The long-term mean heat exchange between the ocean and atmosphere is balanced by meridional advection of heat from low latitudes into the marginal sea. This balance is maintained by the mean transport in the boundary current and the change in temperature between the inflowing and outflowing currents. It is assumed, and found numerically, that the eddy heat flux between the marginal sea and the open ocean is small. The temperature of the water flowing out of the marginal sea is reduced due to heat loss from the boundary current into the basin interior and directly from the boundary current into the atmosphere. In nondimensional form, the meridional heat flux across the sill (or more generally across a specific latitude) Q_{sill} is written as

$$Q_{sill} = \Delta T(\Delta T - \Delta S) + (PL/A)(2\mu/\epsilon)[1 - T' \sin(\omega t)], \tag{2}$$

where P is the perimeter of the marginal sea, L is the width of the sloping topography, and A is the surface

area of the interior of the marginal sea. The dimensional version of this equation can be found in the appendix. The heat flux is nondimensionalized by the amount of heat it would take to change the temperature of the convective basin by an amount T^* over the eddy flushing time scale τ (defined in the appendix). The first term represents the exchange of heat between the boundary current and the interior convective region. The second term is the heat loss directly from the boundary current to the atmosphere, where for simplicity it has been assumed that the boundary current temperature is constant at the inflowing temperature all the way around the marginal sea. This is a good approximation for $\epsilon \ll 1$, which is appropriate for the Labrador Sea and Lofoten basin (Spall 2012). This will slightly overpredict the heat flux across the sill and into the atmosphere because the boundary current will cool as it encircles the basin, reducing the heat exchange with the atmosphere. However, for the low-frequency, strong, eddy forcing regime most representative of the North Atlantic marginal seas, the variability in heat flux is dominated by the interior so this error is small.

The variation in the heat loss to the atmosphere results from air–sea exchange in both the basin interior and over the boundary current. This may be written in nondimensional form as

$$Q_{surf} = (2\mu/\epsilon)[1 - \Delta T - T' \sin(\omega t)]$$
$$+ (PL/A)(2\mu/\epsilon)[1 - T' \sin(\omega t)]. \tag{3}$$

The first term represents air–sea exchange in the basin interior, and the second term is heat loss from the boundary current to the atmosphere.

The heat loss to the atmosphere is shown in Fig. 3a as a function of forcing frequency and $2\mu/\epsilon$. Heat loss is a strong function of the relative strength of restoring compared to eddy fluxes $2\mu/\epsilon$. When $2\mu/\epsilon \ll 1$, the heat loss from the interior dominates heat loss from the
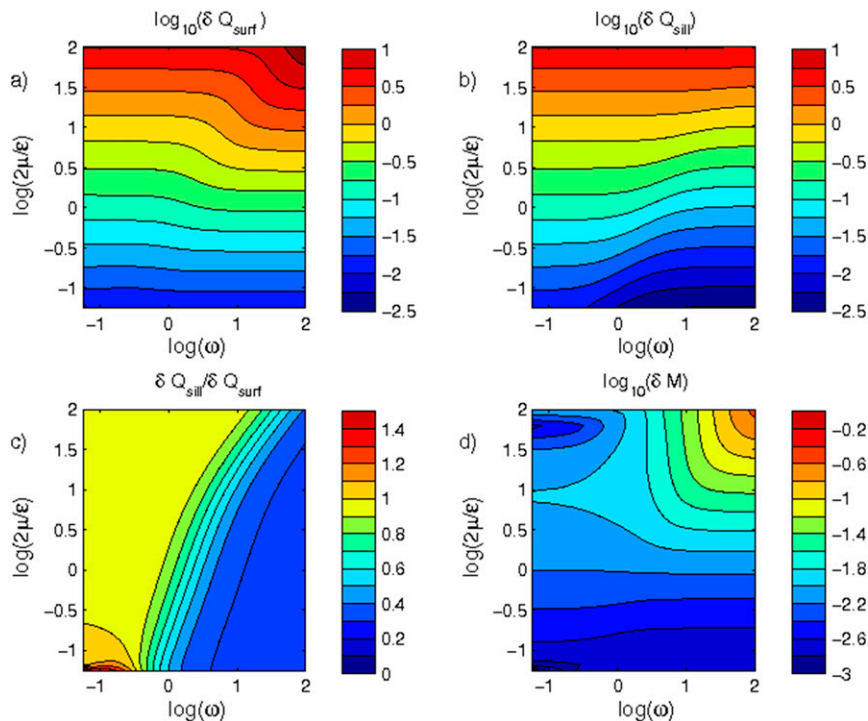
FIG. 3. Nondimensional amplitude of the variability in (a) surface heat flux in the marginal sea; (b) meridional heat flux at the sill latitude; (c) ratio of meridional heat flux to surface heat flux; and (d) meridional overturning circulation at sill latitude.

boundary current at low frequencies, but they are of similar magnitude at high frequencies. However, at low frequencies and weak eddy fluxes, where $2\mu/\epsilon \gg 1$, the heat loss is dominated by the boundary current. In this regime, the interior of the basin is cold and so the air–sea heat flux, which is proportional to the air–sea temperature difference, is small. At high frequencies, once again both terms contribute, which is why the heat flux variability is the largest for strong restoring and high frequencies.

The variation in the meridional heat flux across the sill is shown in Fig. 3b. Again the heat flux is most sensitive to $2\mu/\epsilon$, but we now see a decrease in meridional heat flux for strongly eddying regimes and high-frequency forcing. The magnitude of the second term in (2) is independent of ω, but the first term gets larger at lower frequencies. This is the eddy exchange that gets larger as the baroclinic shear between the boundary current and the interior increases at low frequencies.

In equilibrium, the two heat fluxes balance, as can be inferred from (1). However, for time-dependent forcing the heat loss to the atmosphere will generally not balance the heat transport across the sill, the difference resulting in a change in the temperature of the convective water mass in the basin interior. Both of the heat flux components are nearly out of phase with the atmospheric

temperature, so significant heat storage arises primarily as a result of differences in the amplitude of the meridional heat flux compared to the air–sea heat flux. The ratio of these two fluxes is shown in Fig. 3c. At low frequencies, their amplitudes are nearly equal, indicating little heat storage in the basin interior. In this regime, the circulation is nearly always in balance with the atmosphere because the eddy fluxes have ample time to adjust to the changing atmospheric temperature. There is a local maximum at low frequencies and strong eddy fluxes, which we will return to in section 3. However, at high frequencies, roughly defined as $\omega > 2\mu/\epsilon$, the variability in the meridional heat flux becomes much less than the variability in exchange with the atmosphere. This indicates that the marginal sea buffers change in the local heat flux in the marginal sea from being communicated to the rest of the ocean. This is again indicative of a local, one-dimensional balance in this regime. Over long time scales heat anomalies would be advected out of the basin, but if the atmospheric forcing changes sign on frequencies greater than $2\mu/\epsilon$ then the anomalous heat simply goes back into the atmosphere.

Another quantity of interest is the MOC forced by buoyancy loss in the marginal sea. The loss of buoyancy requires that the outflowing boundary current be more barotropic than the inflowing boundary current in order

to maintain a geostrophic balance (Spall 2010, 2012; Cenedese 2012). This Eulerian measure of the MOC is simply an integral of the vertical velocity over the horizontal extent of the marginal sea. In this layered representation the maximum downwelling takes place at depth $0.5H_S$, where H_S is a sill depth, and is equal to the amount of baroclinic geostrophic transport in the boundary current that is lost due to the reduction in the horizontal density change between the boundary current and the interior. This can be written in nondimensional form as

$$M = 0.5\epsilon\Delta\rho + (PL/A)(\mu/\Delta\rho)[1 - T'\sin(\omega t)]. \quad (4)$$

The dimensional form is given in the appendix. This transport is scaled by the geostrophic transport that would balance a change in temperature of T^* over a depth H_S. This can be considered as the maximum geostrophic transport that the system can support. As for the heat flux terms, the MOC is driven by buoyancy loss in the interior (first term) and buoyancy loss from the boundary current (second term).

The variability of the MOC results from both direct variability in the atmospheric temperature over the boundary current (last term on the right-hand side) and changes in $\Delta\rho$ that result from changes in the atmospheric temperature (first term and coefficient of the second term). Note that the first term and the coefficient of the second term will be out of phase with each other because the second term is proportional to $\Delta\rho^{-1}$. The amplitude of the variability of the MOC is shown in Fig. 3d. There are three regimes: strong eddy forcing ($2\mu/\epsilon \ll 1$), weak eddy forcing and low frequency ($\omega \ll 1$), and weak eddy forcing and high frequency ($\omega \gg 1$). For strong eddy forcing, the variability of the MOC is only weakly dependent on frequency. This is because $\Delta\rho$ does not vary strongly due to damping by the eddy fluxes. As a result, the variability of the MOC is dominated by the last term, the direct forcing from the atmosphere on the boundary current. For weak eddy fluxes the MOC variability remains small at low frequencies. This is a little surprising since ΔT (and $\Delta\rho$) is large in this regime (Fig. 1a). However, there is a similar variation in the coefficient of the second term, proportional to $\Delta\rho^{-1}$ that is out of phase and to a large degree cancels the variation in the first term. However, at high frequencies $\Delta\rho$ becomes 90° out of phase with T' and thus does not compete with the boundary term. As a result, the largest variability in the MOC is found in the weak eddy, $\omega \approx 2\mu/\epsilon$ regime. The transition between these regimes and the quantitative magnitudes of the MOC will depend on the specific model parameters, in particular the relative area of the boundary current compared to the interior, but similar regimes are found.

c. Linearized solutions

The equations derived and solved above provide some clarity into the important parameters governing the behavior of the convective sites but they remain a set of coupled, nonlinear equations. Further simplification, and closed-form analytic solutions, can be obtained in the limit that the perturbations induced by fluctuations in the atmospheric temperature are small compared to the mean state: $\delta T \ll \Delta T_0$ and $\delta S \ll \Delta S_0$. Substituting $\Delta T = \Delta T_0 + \delta T$ and $\Delta S = \Delta S_0 + \delta S$ into (1) and retaining only the leading-order perturbation terms, the governing equations are now linear and uncoupled:

$$\frac{d\delta T}{dt} + C_1\delta T - 2\mu/\epsilon T'\sin(\omega t) = 0, \quad \text{and} \quad (5a)$$

$$\frac{d\delta S}{dt} + C_2\delta S + \Delta S_0\delta T = 0. \quad (5b)$$

The constants C_1 and C_2 are defined as

$$C_1 = 2\Delta T_0 - \Delta S_0 + 2\mu/\epsilon, \quad C_2 = \Delta T_0 - 2\Delta S_0. \quad (6)$$

The changes in temperature are forced by the anomalous atmospheric temperature, and the changes in salinity are forced by δT, the change in the temperature of the convective region through the eddy flux of the mean salinity gradient ΔS_0. These equations neglect the influence of δS on the eddy flux of temperature. While this is generally a good approximation because $\delta S \ll \delta T$ (Fig. 1), it will be shown that this is not a good assumption for very low-frequency regimes.

The solution for sinusoidally varying forcing in which the initial state is equal to the steady solution can be written as

$$\delta T_{\text{LE}} = \frac{(2\mu/\epsilon)T'}{(C_1^2 + \omega^2)^{1/2}}\sin(\omega t + \phi_T), \quad \phi_T = \tan^{-1}(-\omega/C_1),$$

$$(7)$$

and for salinity

$$\delta S_{\text{LE}} = \left(\frac{C_3^2 + C_4^2}{C_2^2 + \omega^2}\right)^{1/2} S_0 \sin(\omega t + \phi_S),$$

$$\phi_S = \tan^{-1}\left(\frac{C_3\omega + C_2 C_4}{C_4\omega - C_2 C_3}\right), \quad (8)$$

where the subscript LE represents the linearized equations, and the constants C_3 and C_4 are defined as

$$C_3 = \frac{(2\mu/\epsilon)C_1 T'}{C_1^2 + \omega^2}, \quad C_4 = \frac{(2\mu/\epsilon)\omega T'}{C_1^2 + \omega^2}. \quad (9)$$

One can also represent transitions from one mean state to another mean state forced by a shift in the mean
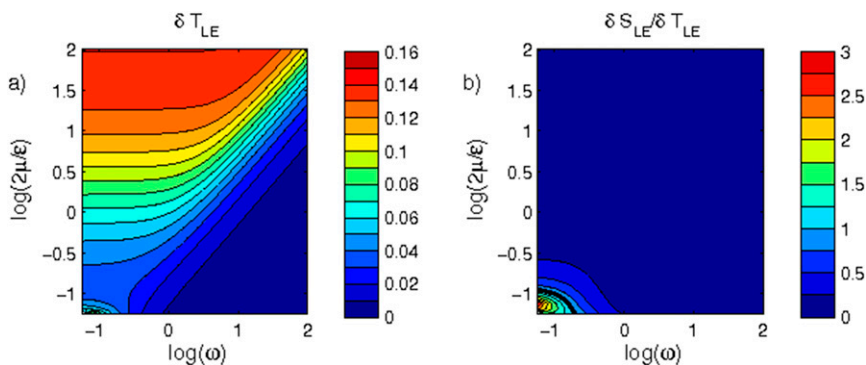
FIG. 4. As in Fig. 1, but for the closed-form analytic solutions (7) and (8).

value of T_a. Yasuda and Spall (2015) consider such solutions for changes in the mean precipitation. They are characterized by an exponential adjustment with an e-folding time scale of the eddy flushing time scale (see also Straneo 2006). However, we will consider only periodic variations in T_a for the remainder of the paper.

The results from this linearized approximation compare very closely with that from the fully coupled non-linear equations, as shown in Fig. 4. The only region of significant disagreement is in the lower-left region of the figure, the low-frequency, strong eddy regime. This is due to the neglect of salinity fluctuations on the baroclinic shear and resulting eddy fluxes, as will be discussed more fully below.

The real utility of this linearized solution is in understanding the limits of the behavior. First, consider low frequency such that $\omega \ll 2\mu/\epsilon$. For weak eddies (or strong restoring to the atmospheric temperature), the amplitude of the temperature variability approaches T' and the phase ϕ_T approaches zero. The salinity in this limit approaches $\Delta S_0 T'/\Delta T_0$ and $\phi_S = -180°$, so the ocean is in an essentially quasi-steady balance with a warm, fresh ocean coinciding with a warm atmosphere. In the limit of strong eddies, so that $2\mu/\epsilon \ll 1$, the variability of the temperature of the convective water mass is

$$\delta T = \frac{\mu T'}{\epsilon \Delta T_0} \ll T'. \tag{10}$$

In this limit, the eddies act to reduce the variability of the convective water mass compared to the case with a more stable boundary current. The eddies always try to bring the ocean back to its equilibrium state.

The salinity variability in this limit is given by

$$\delta S \approx \frac{\Delta S_0}{\Delta T_0 - 2\Delta S_0} \delta T. \tag{11}$$

As long as $\Delta T_0 \gg \Delta S_0$, $\delta S \ll \delta T$, as is generally found in Fig. 4. However, for sufficiently strong precipitation,

$\Delta S_0 \to 0.5\Delta T_0$, which is the condition for which there are no steady convective solutions (Stommel's haline collapse; Spall 2012). As haline collapse is approached, the variability in salinity becomes larger than that for temperature, and it can no longer be neglected as in the linearized theory. This large variability arises because the restoring of salinity in the interior due to eddy fluxes is very weak, which allows the continuous surface precipitation to accumulate large freshwater anomalies at very low frequencies.

In the limit of high-frequency forcing, where $\omega \gg 2\mu/\epsilon$, the temperature and salinity variability are

$$\delta T \to \frac{2\mu/\epsilon}{\omega}T' \ll T', \quad \delta S \to \frac{2\mu/\epsilon}{\omega^2}\Delta S_0 \ll \delta T. \tag{12}$$

In this limit the variability of both temperature and salinity are much less than that of the atmosphere, and salinity variance is much less than temperature variance for $\omega \gg 1$. In this regime, the forcing from the atmosphere changes so rapidly that the ocean does not have time to significantly respond, either by providing heat and salt from the boundary current via lateral eddy fluxes or by changing the local heat content of the convective water mass in the interior.

The ocean response to variations in atmospheric temperature differs from that due to variations in precipitation primarily by the introduction of the atmospheric restoring term, represented by $2\mu/\epsilon$ in the definition of C_1. The equivalent constant for the precipitation-forced system is $\Delta T_0 - \Delta S_0$ (Yasuda and Spall 2015). In the weakly eddying regime, $2\mu/\epsilon \gg 1$, and it dominates the terms due to eddy fluxes $2\Delta T_0 - \Delta S_0$. For strong eddy fluxes, the amplitude of the ocean response is determined by $2\Delta T_0 - \Delta S_0$, which is similar to the eddy flushing frequency of the basin $\Delta\rho_0 = \Delta T_0 - \Delta S_0$. The terms ΔT_0 and ΔS_0 are determined by $2\mu/\epsilon$, and thus the amplitude remains controlled by this parameter. The larger the density difference between the boundary current and the interior, the larger the eddy

fluxes, and the smaller the oceanic response to variations in T_a. The ocean accumulates (or loses) as much anomalous heat as can be absorbed in the time it takes for eddies to flush the basin.

3. Comparisons with an eddy-resolving numerical model

The simplified two-box model for a convective region provides a compact set of equations and, in the limit of small perturbations, closed-form analytic solutions. However, several assumptions were required in order to derive these equations, and it remains to be seen whether or not the basic insights provided by this model carry over to a dynamically more complete system. Key approximations of the theory include parameterization of the eddy heat and salt fluxes, homogeneous interior and boundary current, and neglect of wind forcing. The predictions from the theory are now compared to output from a series of idealized numerical model calculations. The model explicitly resolves mesoscale eddies and baroclinic and barotropic instabilities, represents stratification, contains the barotropic mode, and includes wind forcing.

a. Model configuration

The model used is the MITgcm primitive equation model (Marshall et al. 1997). It solves the primitive equations of motion on a staggered C grid in the horizontal and depth coordinates in the vertical, including a partial cell treatment of the bottom topography. The model configuration closely follows that of Spall (2012) and Yasuda and Spall (2015). The domain is 1000 km in zonal extent and 2000 km in meridional extent (Fig. 5). The maximum bottom depth is 2000 m, and there is topography around the perimeter of the domain that slopes upward to 50-m depth over a width of 140 km. This slope is steeper around the northern end of the domain in order to provide a region of stronger baroclinic instability and exchange between the boundary current and the interior, as is found in the Labrador Sea and the Lofoten basin (Spall 2010). There is also a sill that extends up to 1000-m depth located at 1200-km latitude. The horizontal grid spacing is 5 km, and there are 30 levels in the vertical ranging from 25 m thick at the surface to 200 m thick below 1800 m. The typical internal deformation radius based on the sill depth and the density anomaly of the convective water mass is $O(25)$ km and well resolved by the model grid.

The model is forced at the surface with a restoring of the uppermost model temperature with a time scale of 120 days (or 20 days) toward an atmospheric temperature whose mean $\overline{T}_a$ is indicated in Fig. 5 by the colors.
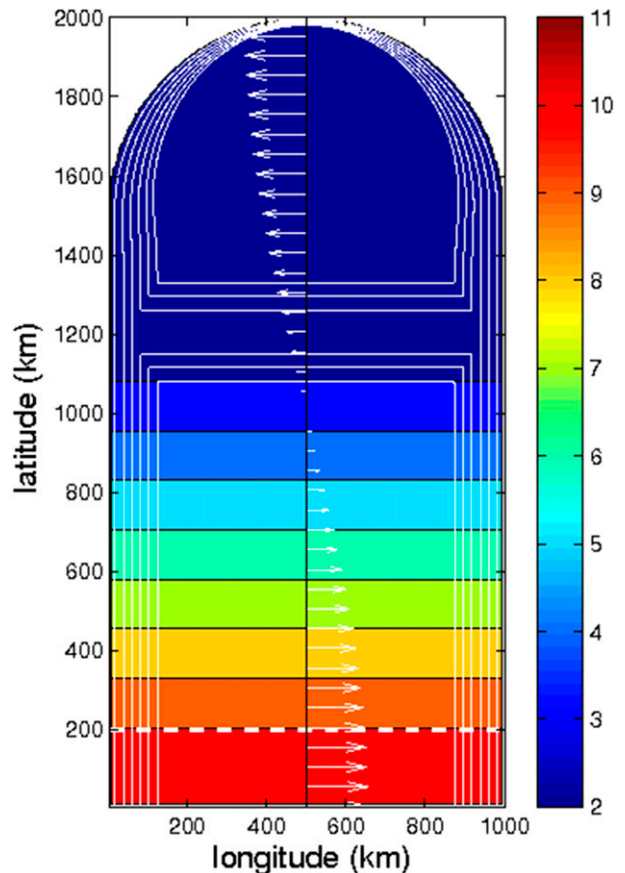

FIG. 5. Model domain and forcing. Mean atmospheric temperature is given by the colors, bottom topography is given by the white contours (contour interval 300 m), and wind vectors are indicated by the white vectors (independent of longitude).

There is also a prescribed virtual freshwater flux that is zero south of the sill at $y = 1200$ km and constant at -2×10^{-8} m s^{-1} north of the sill. A zonal wind stress $\tau^x = \tau_0 \sin(\pi y/L)$ is applied with $\tau_0 = 0.1$ N m^{-2} and $L = 1200$ km (white vectors). The model temperature and salinity are also restored toward a warm, salty uniformly stratified profile between $y = 0$ and $y = 200$ km with a time scale of 60 days. The Brunt–Väisälä frequency is 1.7×10^{-6} s^{-2} with a surface temperature of 10°C and uniform salinity of 35, giving a first-mode baroclinic deformation radius of 20 km. This provides whatever heat and salt are required to balance the surface forcing over the model domain and allows for equilibrium solutions to be obtained in relatively short time. The spinup here is controlled by the eddy advective time scale instead of the much longer vertical diffusion time scale required by models that close the meridional overturning circulation by diapycnal mixing. The advantage of this approach is that equilibrium solutions are obtained on decadal time scales instead of

century time scales. The disadvantage is that there is no feedback between the processes at high latitudes and the water mass properties advected northward from low latitudes.

The model was started at rest and spun up with steady forcing for a period of 50 yr, by which time it has arrived at a statistically steady state. The dependence of the steady-state properties of the convective water mass, heat transport, and MOC on the model parameters is discussed in Spall (2012). A snapshot of the model SST and horizontal velocity vectors after 50 yr is shown in Fig. 6. The basic circulation is representative of high-latitude convective regions such as the Labrador Sea, the Lofoten basin, or the Greenland Sea (Marshall and Schott 1999). There is a region of cold, fresh, weakly stratified water in the basin interior surrounded by a cyclonic boundary current of warm, salty water. The warm water flows into the marginal sea along the eastern boundary and exits along the western boundary. The outflowing water is colder and fresher than the inflowing water, as it must be to balance heat and freshwater exchange with the atmosphere, but it is not as cold or fresh as the water in the basin interior.

As an example of the forced time-dependent response, the atmospheric temperature over the marginal sea was varied as $T_a = \overline{T_a} + T'^* \sin(\omega^* t^*)$, where $T'^* = 1°C$, $\omega^* = 2\pi/20$ yr, and t^* is dimensional time. This periodic forcing with the 20-yr period was applied for 60 yr or three periods of forcing. The resulting temperature and salinity of the convective water mass and the maximum of the meridional overturning circulation at the latitude of the sill are shown in Fig. 7. The atmospheric temperature is shown in Fig. 7a, scaled for comparison with the phase of the ocean response. The temperature of the convective water mass varies by about 0.2°C or 20% of the change in atmospheric temperature. The ocean lags the atmosphere slightly with the peak ocean temperature found after the peak atmospheric temperature but before the atmosphere has turned anomalously cold. This indicates that lateral exchange from the boundary current via eddies is influencing the properties of the convective water. The temperature of the convective water predicted by the theory (1) is shown by the dashed line. For this case, based on the numerical model parameters, $2\mu/\epsilon = 0.175$, $\gamma = -0.02$, and $\epsilon = 0.13$. The mean temperature is about 0.5°C colder than that found in the model, which reflects a small error in the steady theory. However, the variability predicted by the theory compares very well with the numerical model both in terms of phase and amplitude.

The salinity in the interior shows only weak variability of $O(0.002)$ that is not well represented by a sinusoidal
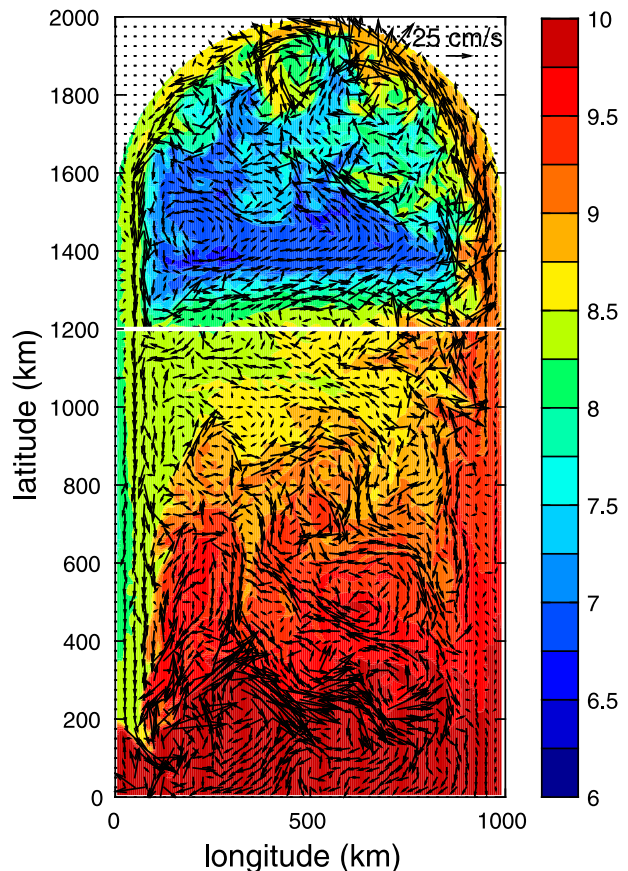

FIG. 6. Sea surface temperature at the end of the 50-yr spinup period along with horizontal velocity vectors (every fifth grid point). A reference velocity scale of 25 cm s⁻¹ is given in the upper-right corner of the figure. The sill latitude is indicated by the white line.

variation with a period of 20 yr. The magnitude of the variation is of the same order of magnitude as that predicted by the theory (dashed line Fig. 7b), but there is additional variability on both longer and shorter time scales. This indicates that the natural internal variability of the salinity is as large as the expected forced variability, and so the theory is unable to reproduce the model results. This enhanced low-frequency variability in salinity compared to temperature is likely a red spectrum response to random forcing by eddies from the boundary current and the lack of damping by the atmosphere for salinity.

The maximum value of the meridional overturning circulation at the latitude of the sill is shown in Fig. 7c. The mean MOC is approximately 2 Sverdrups (Sv; 1 Sv ≡ 10^6 m³ s⁻¹) and of a similar order of magnitude to that found in the Labrador Sea and the Nordic Seas (e.g., Pickart and Spall (2007). The strength of the MOC varies by about 10% in response to the changing atmospheric temperature. The phase is such that the MOC is strongest when the atmosphere is coldest. The theory
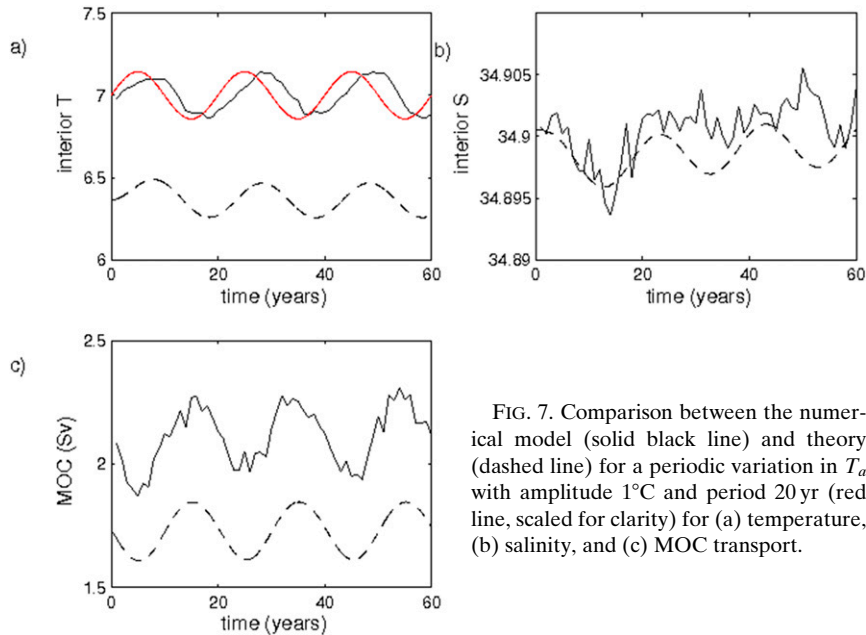
FIG. 7. Comparison between the numerical model (solid black line) and theory (dashed line) for a periodic variation in T_a with amplitude 1°C and period 20 yr (red line, scaled for clarity) for (a) temperature, (b) salinity, and (c) MOC transport.

slightly underpredicts the mean model MOC but compares well with the variability.

These results suggest that the theory is at least partly supported by the numerical model results. However, the real strength of the theory, and purpose of the study, is to understand how the magnitude and phase of the ocean response depends on the frequency of forcing and configuration of the ocean basin. A comparison between the theory and the numerical model is now carried out in which the frequency of forcing is varied. Two basic configurations are considered: one in a strong eddying regime (atmospheric restoring time scale 120 days; $2\mu/\epsilon = 0.175$) and one in a weak eddying regime (atmospheric restoring time scale 20 days; $2\mu/\epsilon = 1.2$).

b. Strong eddy regime: $2\mu/\epsilon = 0.175$

A series of numerical model calculations is now carried out in which the domain and forcing are the same as in the above example, but the period of forcing is varied from 1 to 400 yr. In cases with periods less than 100 yr, the forcing is repeated for three cycles. For cases with periods of 100, 250, and 400 yr, only one cycle is run and the model grid spacing was increased from 5 to 10 km for computational efficiency. This is still less than half the internal deformation radius.

The amplitude of the variability in each of the diagnosed quantities is determined by the amplitude of a Fourier transform of the time series at the forcing frequency. For most cases, this closely represents the actual evolution, indicating that the forced response dominates the internal variability. In a few cases, the internal variability dominates (such as for salinity in Fig. 7b); these will be mentioned

explicitly below. The phase is diagnosed from the phase of this Fourier mode relative to the forcing.

The amplitude of the variability in δT, δS, and δM diagnosed from the model is compared to that predicted by the theory in Fig. 8. Each of these quantities is nondimensionalized by the same scaling used in the theory. The agreement for temperature is reasonably good (solid line, circles). At high frequency, the variability of the temperature is very small, while it increases as the frequency of forcing decreases, as expected from the linear decoupled theory. The transition from high to low frequency occurs around $\omega = 1$, although the increase is spread over an order of magnitude in forcing frequency. The amplitude peaks near $\omega = 0.5$ and then decreases at lower frequency, consistent with the theory. The maximum amplitude of the variability in ocean temperature, approximately 0.03, is much less than the amplitude of the variability in atmospheric temperature, 0.14, due to the damping influence of the eddies.

The amplitude of the variability in salinity is indicated by the dashed line (theory) and squares (model). Again we find low amplitudes at high frequency and increasing amplitude as the frequency of forcing decreases. The theory overpredicts the amplitude by more than a factor of 2 at the lowest frequency, but the increase found in the model occurs in the same frequency range. It is not clear why there is such a large discrepancy between model and theory amplitude at low frequencies.

The variability in the MOC is given by the dotted–dashed line and triangles. The theory predicts very little change in amplitude with frequency, roughly in
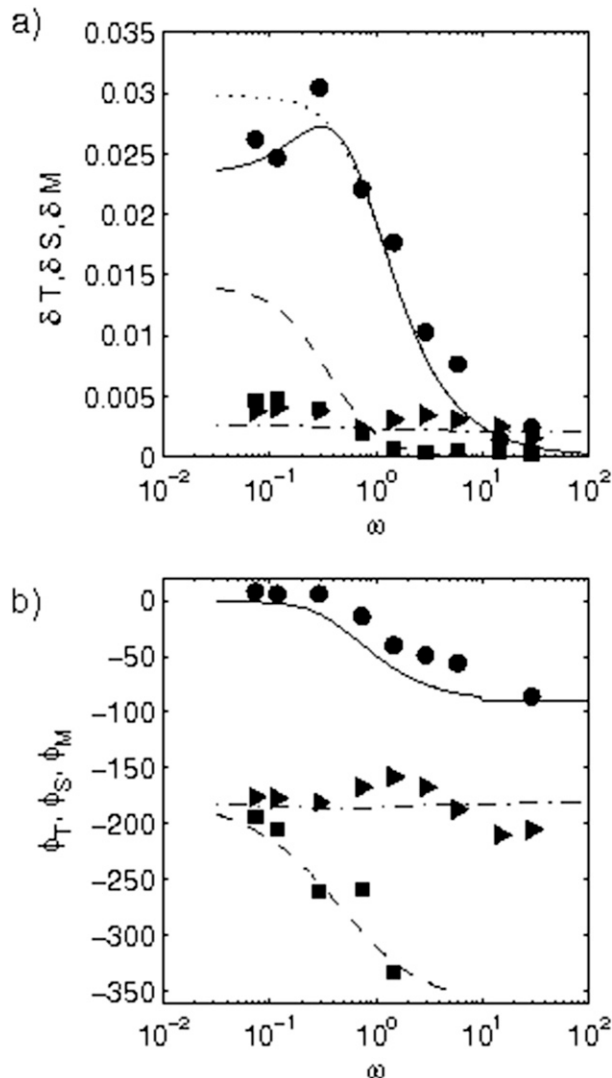
FIG. 8. Comparison between the numerical model (symbols) and theory (lines) over a range of forcing frequency for the strongly eddying regime. (a) Nondimensional variance amplitude and (b) phase for temperature (solid line, circles), salinity (dashed line, squares), and MOC (dotted–dashed line, triangles). The dotted line is the linear theory (7).

accord with the results of the model. This is somewhat surprising since the density of the convective water mass shows a strong dependence on the frequency of forcing with large fluctuations at low-frequency forcing but is consistent with the theory and the dominance of the time-dependent boundary forcing term in (4).

The phase of the variability in T, S, and M is shown in Fig. 8b. There is generally good agreement between the model and theory for each of these quantities. At high frequencies the temperature lags the atmosphere by 90°, as would be expected for a one-dimensional balance in which lateral eddy fluxes from the boundary current are

not important. This transitions to be in phase with the atmosphere at low frequency. In this regime, the eddies are sufficiently strong to maintain a near-steady balance with the atmospheric forcing. Salinity is in phase with the atmosphere at high frequency (freshwater when the atmosphere is warm) and transitions to be 180° out of phase at low frequency.[1] It is this change in phase at low frequencies that causes the linear decoupled theory to depart from the full theory at low frequencies (the linear theory is given by the dotted line in Fig. 8a). The linear theory neglects the influence of δS on the eddy flux from the boundary current. At low frequency, the amplitude of δS increases, making salinity more important, and it becomes out of phase with δT. However, since $\delta\rho = \delta T - \delta S$, an out of phase salinity reinforces the density contrast arising from the temperature variability. This means that the eddy fluxes will be larger than predicted by the decoupled theory, resulting in depressed variance of temperature. The MOC is nearly out of phase for all frequencies in both the model and the theory so that the MOC is weak when the atmosphere is warm. This again results from the dominance of the boundary forcing term in driving the MOC.

The amplitude and phase of variations in the meridional heat flux at the sill latitude and the surface heat flux north of the sill are shown in Fig. 9. The amplitude at low frequencies is nearly equal and close to that predicted by the theory. Again this is as expected for the regime in which the atmosphere varies so slowly that the ocean is always in a nearly steady state with the atmosphere. However, as the frequency increases, the variance amplitude of the meridional heat flux decreases significantly, while the variance amplitude of the surface heat flux actually increases slightly (see also Fig. 3). The model and theory agree reasonably well, although there is some variability in the amplitude of the meridional heat flux in the model at high-frequency forcing.

Both components of heat flux are nearly out of phase with the atmosphere, as expected (warm atmosphere, less heat flux). Again the model and theory agree well. There is a slight shift in phase of the meridional heat flux for frequencies of $O(1)$ in both the model and the theory, but in all cases, the lag is close to 180°. This means that there is essentially no heat storage on the time scale of the forcing at low frequencies, but nearly all the heat exchange at the surface remains within the marginal sea at high-frequency forcing.

---

[1] The phase ϕ_S is not shown for cases in which the percent of the variance in the model that is reproduced by the Fourier mode at the forcing frequency is less than 10% since the time dependence is dominated by internal variability.
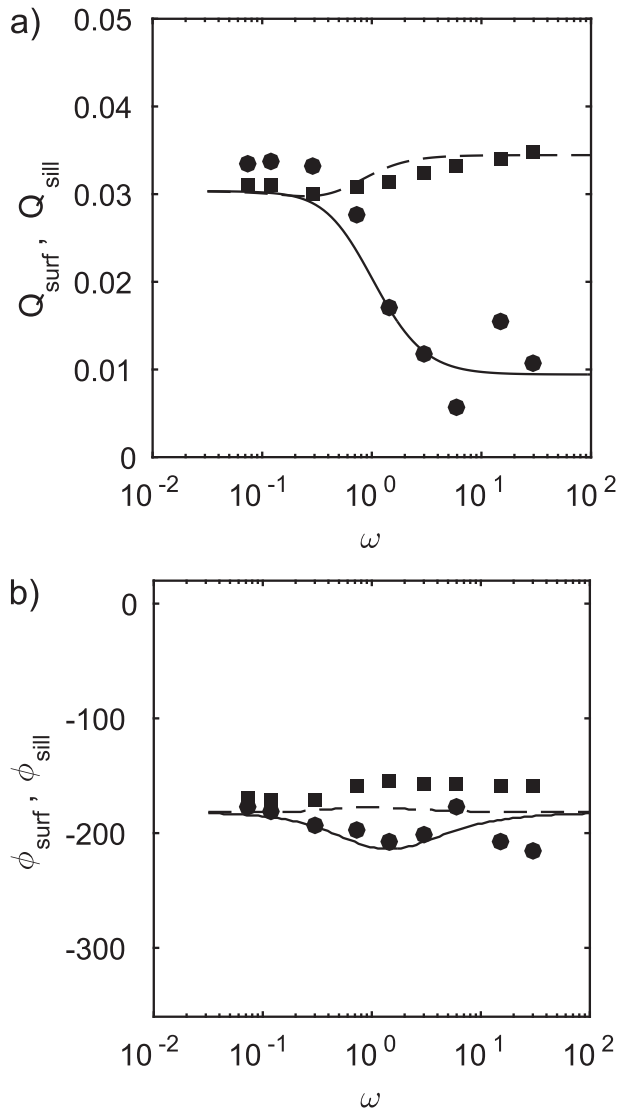
a)

b)

FIG. 9. Comparison between the numerical model (symbols) and theory (lines) over a range of forcing frequency for the strongly eddying regime. (a) Nondimensional variance amplitude and (b) phase for meridional heat flux at the sill latitude (solid line, circles) and surface heat flux (dashed line, squares).

c. Weak eddy regime: $2\mu/\epsilon = 1.2$

A second set of numerical model calculations was carried out that are the same as the first set except with the restoring time scale to the atmospheric temperature was reduced to 20 days. This increases the nondimensional parameter $2\mu/\epsilon$ to 1.2 (it increases by slightly more than a factor of 6 because the inflowing temperature decreases, causing T^* to increase).

The general behavior is similar to that found previously, but there are important differences (Fig. 10). The amplitude of the temperature variance at low frequencies is more than twice as large as in the previous strongly

eddying case and well predicted by the theory. The linear theory overpredicts the variability, although there is no suppression of variability at very low frequencies. The model predicts an increase in salinity variance at low frequencies, but it is still less than is predicted by the theory. The MOC amplitude remains relatively insensitive to forcing frequency, although there is some increase at very low frequencies that is not predicted by the theory. The transition from low-frequency behavior to high-frequency behavior takes place at higher frequency than it did for the weaker surface restoring cases, as expected for larger $2\mu/\epsilon$.

The phase relationships for δT, δS, and δM are generally well predicted by the theory and similar in character to the strongly eddying regime (Fig. 10b). There is also a similar level of agreement between the model and the theory for the meridional heat flux and air–sea heat flux as found in Fig. 9 (not shown).

d. More complex T_a

The previous forcing with a single frequency of variability in T_a allows for linearized analytic solutions and clearly demonstrates how the ocean response depends on the frequency of forcing. A more general and realistic variation in T_a is attained by a superposition of three different forcing frequencies as

$$T_a = \overline{T}_a + T_1'^* \sin(\omega_1^* t^*) + T_2'^* \sin(\omega_2^* t^*) + T_3'^* \sin(\omega_3^* t^*).$$ (13)

As an example, we take $\omega_1^* = 2\pi/60\,\text{yr}$, $\omega_2^* = 2\pi/20\,\text{yr}$, and $\omega_3^* = 2\pi/7.50\,\text{yr}$ with $T_1'^* = 0.75°C$, $T_2'^* = 0.75°C$, and $T_3'^* = 0.5°C$. The resulting anomaly in the atmospheric temperature over 120 yr is shown in Fig. 11 by the red line (offset by $-0.25°C$ for clarity). The numerical model was run with this surface forcing and $2\mu/\epsilon = 0.175$. The resulting temperature and salinity anomalies of the convective water mass are indicated by the black lines in Figs. 11a and 11b. The temperature and salinity predicted by the theory are shown by the green lines. There is close agreement for temperature, especially at frequencies of more than a few years. There is some discrepancy around year 40, where the model is colder than the theory, but this difference is not found 60 yr later (the forcing repeats every 60 yr). This is an indication that the model retains a memory of its initial state even after 40 yr. The high-frequency variability in T_a does not significantly imprint on ocean temperature, as expected from the theory above. There is also a slight phase shift between extremes in T_a and extremes in ocean temperature, also consistent with the theory.

The amplitude of the low-frequency variability of salinity is reproduced by the theory, although there is a slight phase shift compared to the model. There is
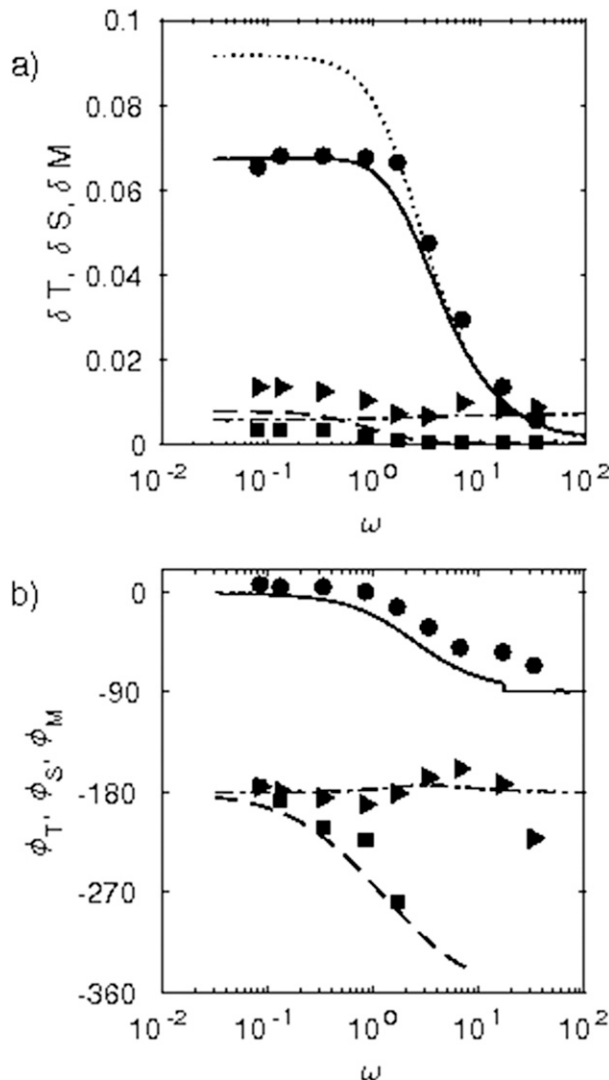
FIG. 10. As in Fig. 8, but for the weakly eddying regime.

considerable variability in the model salinity at frequencies less than 10 yr that are not reproduced by the theory. This is presumably due to natural internal variability. A similar dominance of internal variability for salinity at high frequencies was found by Yasuda and Spall (2015). These results indicate that for these relatively weak variations in T_a, the ocean response is essentially linear and allows for the ideas derived from the single-frequency forcing considered above to be applied to more general and complex variations in the atmosphere.

4. Summary

The ocean response to variations in atmospheric temperature over a convective basin was considered using a simple analytical model and a series of idealized

numerical model calculations. The influence of such variability is characterized by the amplitude and phase of the variability induced in the convective water mass properties, the ocean heat flux into the marginal sea and into the atmosphere, and the meridional overturning circulation. The theory is based on a two-box model of the marginal sea system: a convective interior and a buoyant cyclonic boundary current. The exchange of properties between the two regions is controlled by eddy fluxes arising from baroclinic instability of the boundary current. This idealization gives rise to a pair of coupled, nonlinear algebraic equations for the temperature and salinity anomalies of the convective water mass. In the limit of weak anomalies, a linearization of the equations with sinusoidal forcing allows for closed-form analytic solutions. Consideration of mass, heat, and salt budgets over the whole marginal sea provides for analytic estimates of the meridional heat flux, surface heat flux, and meridional overturning circulations. The primary outcome of this analytic model is the identification of two distinct regimes of behavior defined by the frequency of forcing compared to the response time to local atmospheric forcing. At high-frequency forcing, the system is essentially one-dimensional and responds weakly to atmospheric forcing. At low frequencies, the ocean response is stronger and is regulated by eddy fluxes from the boundary current into the interior. The amplitude of the variability in the ocean generally decreases as eddy fluxes increase. This differs from variability forced by changes in precipitation, which is governed at all frequencies by the lateral eddy flux term because there is no equivalent one-dimensional time scale.

The basic predictions arising from the theory were tested by comparison with an idealized primitive equation numerical model of a convective basin. The model explicitly resolves mesoscale eddies and baroclinic and barotropic instabilities, includes surface heat flux, freshwater flux, and wind forcing. The model also includes the barotropic mode, finite topography, and stratification. Two sets of calculations were carried out, one in a strongly eddying regime and one in a weakly eddying regime. The theory generally compared well with the model, lending support to the basic dynamics drawn from the theory. The analysis has been limited to relatively weak perturbations to the atmospheric temperature such that the system remains in a linear regime and always supports deep convection. However, for sufficiently strong perturbations it is expected that the system could shift into the haline collapse regime in which the interior is too fresh to support deep convection. It remains to be seen whether this results in a permanent transition to the haline mode or the system is able to reinitiate deep convection when the atmosphere transitions to the cold phase.
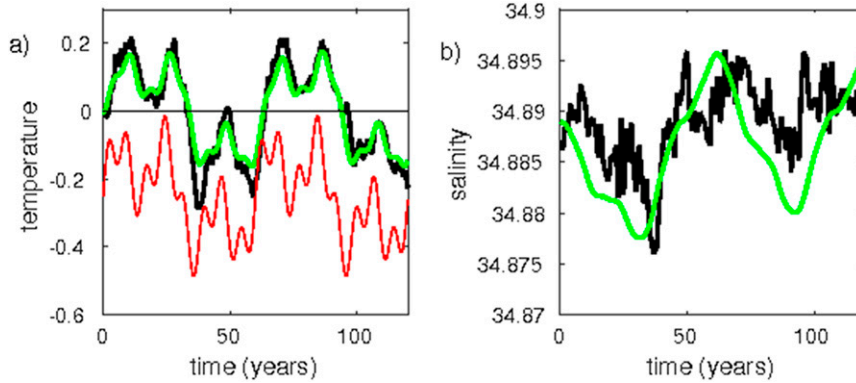
FIG. 11. Convective water mass anomalies for a superposition of three forcing frequencies for T' (red line, offset by -0.25°C). (a) Temperature and (b) salinity; model (black line) and theory (green line).

These results indicate that the ocean response to changes in atmospheric temperature are complex and depend strongly on the geometry of the convective basin and the frequency of the forcing. The amplitude and phase of various oceanic quantities, such as water mass properties, heat flux, and MOC, differ from each other and are generally not trivially related to the change in atmospheric temperature. The theory presented here provides relatively simple guidelines with which to interpret and predict changes in the ocean that are forced by changes in atmospheric temperature.

APPENDIX

The Two-Box Model

The convective basin is assumed to be described by an interior convective region defined by closed geostrophic contours (closed f/h, where f is the Coriolis parameter and h is the bottom depth) and a surrounding region of width L defined by bottom topography that slopes upward to the coast and connects with the ocean to the south (Fig. A1). The governing equations are derived first for the temperature and salinity in the convective region. It is assumed that the mean flow is along geostrophic contours so that the exchange of heat and salt between the interior region and the surrounding boundary current is entirely due to eddies. The equations for

heat and salt in the interior are then given by a balance between surface forcing and lateral eddy fluxes. It is assumed that the surface heat flux is proportional to the difference between the ocean temperature in the basin interior T_0 and the atmospheric temperature T_a. Subscripts 1 indicate boundary current values and subscripts 0 indicate basin interior values. The freshwater flux is instead imposed as a constant, independent of the ocean state:

$$H_0 A \frac{dT_0}{dt*} = P H_S c V (T_1 - T_0) - \frac{A\Gamma(T_0 - T_a)}{\rho_0 C_p}, \quad \text{and}$$

(A1a)

$$H_0 A \frac{dS_0}{dt*} = P H_S c V (S_1 - S_0) - A\mathcal{S}E,$$ (A1b)

where H_0 is the depth; A is the area of the convective region; H_S is the depth of a sill that separates the marginal sea from the ocean to the south (could be equal to H_0); P is the perimeter of the convective region; E is the net evaporation minus precipitation; ρ_0 is a reference density; $\mathcal{S}$ is a reference salinity; and C_p is the specific heat of seawater. The eddy tracer fluxes between the boundary current and the interior are parameterized as being proportional to cV times the difference in temperature or salinity between the boundary current and the interior, as derived by Spall (2004). The value $c = 0.007$ is a nondimensional constant that represents the efficiency of lateral eddy fluxes from baroclinically unstable currents. This value is smaller than typical for flat bottom configurations because the sloping bottom stabilizes the boundary current, as discussed in Spall (2004). The velocity scale V is the baroclinic shear in the boundary current driven by the change in density between the boundary current and the interior:
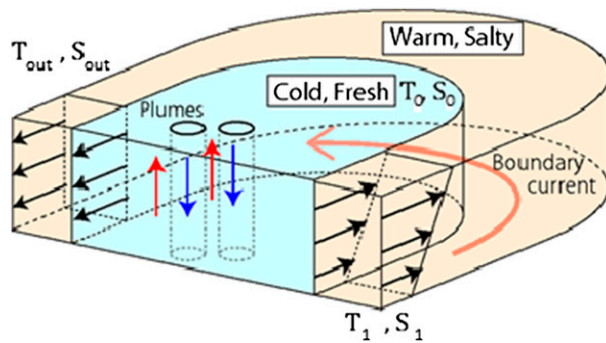
FIG. A1. Schematic of the idealized marginal sea. The basin interior is defined by closed geostrophic contours, and the boundary region is defined by open geostrophic contours. The boundary current is warm and salty; the interior is cold and fresh. Exchange between the two is driven by eddy fluxes resulting from baroclinic instability. The marginal sea is cooled by restoring to a time-dependent atmospheric temperature and freshened by a uniform, constant precipitation. Figure modified from Yasuda and Spall (2015).

$$V = \frac{gH_S}{2\rho_0 f_0 L}[\alpha_T(T_1 - T_0) - \alpha_S(S_1 - S_0)], \quad (A2)$$

where g is the gravitational acceleration; f_0 is the Coriolis parameter (constant); L is the width of the sloping bottom topography under the boundary current; and α_T and α_S are the thermal and haline expansion coefficients.

The meridional heat flux across the sill Q^*_{sill} and the heat exchange with the atmosphere Q^*_{surf} can be written in dimensional form as

$$Q^*_{\text{sill}} = \frac{\rho_0 C_p H_0 A}{\tau T^*}(T_1 - T_0)[(T_1 - T_0) - \alpha_s/\alpha_T(S_1 - S_0)]$$
$$+ PL\Gamma(T_1 - T_a), \quad \text{and}$$
$$(A3a)$$

$$Q^*_{\text{surf}} = \Gamma A(T_0 - T_a) + \Gamma PL(T_1 - T_a). \quad (A3b)$$

The meridional overturning circulation is derived as the amount of vertical transport required to maintain geostrophic balance in the boundary current, which in dimensional form is

$$M^* = \frac{cPgH_S^2}{4L\rho_o f_0}(\rho_1 - \rho_0) + \frac{\Gamma PL\alpha_T}{2\rho_0 C_p(\rho_1 - \rho_0)}(T_1 - T_a). \quad (A4)$$

The difference between the density of the inflowing boundary current and the basin interior is $\rho_1 - \rho_0 = \alpha_T(T_1 - T_0) - \alpha_S(S_1 - S_0)$.

The equations governing the temperature and salinity anomalies can be written in nondimensional form as

$$\frac{d\Delta T}{dt} = -\Delta T(\Delta T - \Delta S) + 2\mu/\epsilon(1 - \Delta T + T'), \quad \text{and}$$
$$(A5a)$$

$$\frac{d\Delta S}{dt} = -\Delta S(\Delta T - \Delta S) - \gamma/4\epsilon. \quad (A5b)$$

The nondimensional temperature and salinity differences are defined as $\Delta T = (T_1 - T_0)/T^*$ and $\Delta S = \alpha_S(S_1 - S_0)/\alpha_T T^*$, where $T^* = T_1 - \overline{T}_a$ and the overbar indicates the time mean. Time is scaled by

$$\tau = \frac{2\rho_0 f_0 LH_0 A}{gcPH_S^2\alpha_T T^*}. \quad (A6)$$

This is the time it would take for eddies to flush the interior of the basin (if the density contrast between the boundary current and the interior were $\alpha_T T^*$), similar to the time scale derived by Straneo (2006). Nondimensional forms for the heat fluxes and meridional overturning strength are given in section 2.

The nondimensional numbers μ, ϵ, and γ are defined as $\epsilon = cP/L$, $\mu = A\Gamma f_0/\alpha_T g C_p H_S^2 T^*$, and $\gamma = 8A\rho_0 f_0 ZS\alpha_S E/gH_S^2\alpha_T^2 T^{*2}$. The parameter ϵ may be thought of as the fraction of the boundary current water that is fluxed into the interior by eddies. The relative strength of precipitation to lateral eddy fluxes of salt is measured by γ and the balance between surface heat flux and lateral eddy fluxes is represented by μ. For a more detailed discussion of these parameters, see Spall (2012). For the calculations in this paper, based on the configuration of the numerical model, $\epsilon = 0.13$ and $\gamma = -0.02$.

REFERENCES

Anderson, D. L. T., and P. D. Killworth, 1977: Spin-up of a stratified ocean with topography. *Deep-Sea Res.*, **24**, 709–732, doi:10.1016/0146-6291(77)90495-7.

Cenedese, C., 2012: Downwelling in basins subject to buoyancy loss. *J. Phys. Oceanogr.*, **42**, 1817–1833, doi:10.1175/JPO-D-11-0114.1.

Cessi, P., and P. Otheguy, 2003: Oceanic teleconnections: Remote response to decadal wind forcing. *J. Phys. Oceanogr.*, **33**, 1604–1617, doi:10.1175/2400.1.

Delworth, T. L., and R. J. Greatbatch, 2000: Multidecadal thermohaline circulation variability driven by atmospheric surface flux forcing. *J. Climate*, **13**, 1481–1495, doi:10.1175/1520-0442(2000)013<1481:MTCVDB>2.0.CO;2.

Grégorio, S., T. Penduff, G. Serazin, J.-M. Molines, B. Barnier, and J. Hirschi, 2015: Intrinsic variability of the Atlantic meridional overturning circulation at interannual-to-multidecadal timescales. *J. Phys. Oceanogr.*, **45**, 1929–1946, doi:10.1175/JPO-D-14-0163.1.

Kawase, M., 1987: Establishment of deep ocean circulation driven by deep-water production. *J. Phys. Oceanogr.*, **17**, 2294–2317, doi:10.1175/1520-0485(1987)017<2294:EODOCD>2.0.CO;2.

Khatiwala, S., and M. Visbeck, 2000: An estimate of the eddy-induced circulation in the Labrador Sea. *Geophys. Res. Lett.*, **27**, 2277–2280, doi:10.1029/1999GL011073.

Lilly, J. M., and P. B. Rhines, 2002: Coherent eddies in the Labrador Sea observed from a mooring. *J. Phys. Oceanogr.*, **32**, 585–598, doi:10.1175/1520-0485(2002)032<0585:CEITLS>2.0.CO;2.

——, ——, F. Schott, K. Lavender, J. Lazier, U. Send, and E. D. Asaro, 2003: Observations of the Labrador Sea eddy field. *Prog. Oceanogr.*, **59**, 75–176, doi:10.1016/j.pocean.2003.08.013.

Lucas, M. A., J. J. Hirschi, J. D. Stark, and J. Marotzke, 2005: The response of an idealized ocean basin to variable buoyancy forcing. *J. Phys. Oceanogr.*, **35**, 601–615, doi:10.1175/JPO2710.1.

Marshall, J., and F. Schott, 1999: Open-ocean convection: Observations, theory, and models. *Rev. Geophys.*, **37**, 1–64, doi:10.1029/98RG02739.

——, C. Hill, L. Perelman, and A. Adcroft, 1997: Hydrostatic, quasi-hydrostatic, and non-hydrostatic ocean modeling. *J. Geophys. Res.*, **102**, 5733–5752, doi:10.1029/96JC02776.

Pedlosky, J., 2006: Time-dependent response to cooling in a beta-plane basin. *J. Phys. Oceanogr.*, **36**, 2185–2198, doi:10.1175/JPO2967.1.

Pickart, R. S., and M. A. Spall, 2007: Impact of Labrador Sea convection on the North Atlantic meridional overturning circulation. *J. Phys. Oceanogr.*, **37**, 2207–2227, doi:10.1175/JPO3178.1.

Spall, M. A., 2004: Boundary currents and water mass transformation in marginal seas. *J. Phys. Oceanogr.*, **34**, 1197–1213, doi:10.1175/1520-0485(2004)034<1197:BCAWTI>2.0.CO;2.

——, 2010: Non-local topographic influences on deep convection: An idealized model for the Nordic Seas. *Ocean Modell.*, **32**, 72–85, doi:10.1016/j.ocemod.2009.10.009.

——, 2012: Influences of precipitation on water mass transformation and deep convection. *J. Phys. Oceanogr.*, **42**, 1684–1700, doi:10.1175/JPO-D-11-0230.1.

——, and R. S. Pickart, 2003: Wind-driven recirculations and exchange in the Labrador and Irminger Seas. *J. Phys. Oceanogr.*, **33**, 1829–1845, doi:10.1175/2384.1.

Stommel, H., 1961: Thermohaline convection with two stable regimes of flow. *Tellus*, **13A**, 224–230, doi:10.1111/j.2153-3490.1961.tb00079.x.

Straneo, F., 2006: On the connection between dense water formation, overturning, and poleward heat transport in a convective basin. *J. Phys. Oceanogr.*, **36**, 1822–1840, doi:10.1175/JPO2932.1.

Yasuda, Y., and M. A. Spall, 2015: Influences of time-dependent precipitation on water mass transformation, heat fluxes, and deep convection in marginal seas. *J. Phys. Oceanogr.*, **45**, 1822–1842, doi:10.1175/JPO-D-14-0147.1.